AMERICAN SOCIETY FOR MICROBIOLOGY | Journal of Virology®

PATHOGENESIS AND IMMUNITY

Lab-Attenuated Rabies Virus Facilitates Opening of the Blood-Brain Barrier by Inducing Matrix Metallopeptidase 8

An Fang,[a,b] Yueming Yuan,[a,b] Fei Huang,[a,b] Caiqian Wang,[a,b] Dayong Tian,[a,b] Rui Zhou,[a,b] Ming Zhou,[a,b] Huanchun Chen,[a,b] Zhen F. Fu,[a,b] Ling Zhao[a,b]

[a]State Key Laboratory of Agricultural Microbiology, Huazhong Agricultural University, Wuhan, China
[b]Key Laboratory of Preventive Veterinary Medicine of Hubei Province, College of Veterinary Medicine, Huazhong Agricultural University, Wuhan, China

An Fang and Yueming Yuan contributed equally to this work. Author order was determined alphabetically.

ABSTRACT Infection with laboratory-attenuated rabies virus (RABV), but not wild-type (wt) RABV, can enhance the permeability of the blood-brain barrier (BBB), which is considered a key determinant for RABV pathogenicity. A previous study showed that the enhancement of BBB permeability is directly due not to RABV infection but to virus-induced inflammatory molecules. In this study, the effect of the matrix metallopeptidase (MMP) family on the permeability of the BBB during RABV infection was evaluated. We found that the expression level of MMP8 was upregulated in mice infected with lab-attenuated RABV but not with wt RABV. Lab-attenuated RABV rather than wt RABV activates inflammatory signaling pathways mediated by the nuclear factor κB (NF-κB) and mitogen-activated protein kinase (MAPK) pathways. Activated NF-κB (p65) and AP-1 (c-Fos) bind to the MMP8 promoter, resulting in upregulation of its transcription. Analysis of mouse brains infected with the recombinant RABV expressing MMP8 indicated that MMP8 enhanced BBB permeability, leading to infiltration of inflammatory cells into the central nervous system (CNS). In brain-derived endothelial cells, treatment with MMP8 recombinant protein caused the degradation of tight junction (TJ) proteins, and the application of an MMP8 inhibitor inhibited the degradation of TJ proteins after RABV infection. Furthermore, an *in vivo* experiment using an MMP8 inhibitor during RABV infection demonstrated that BBB opening was diminished. In summary, our data suggest that the infection of lab-attenuated RABV enhances the BBB opening by upregulating MMP8.

IMPORTANCE The ability to change BBB permeability was associated with the pathogenicity of RABV. BBB permeability was enhanced by infection with lab-attenuated RABV instead of wt RABV, allowing immune cells to infiltrate into the CNS. We found that MMP8 plays an important role in enhancing BBB permeability by degradation of TJ proteins during RABV infection. Using an MMP8 selective inhibitor restores the reduction of TJ proteins. We reveal that MMP8 is upregulated via the MAPK and NF-κB inflammatory pathways, activated by lab-attenuated RABV infection but not wt RABV. Our findings suggest that MMP8 has a critical role in modulating the opening of the BBB during RABV infection, which provides fresh insight into developing effective therapeutics for rabies and infection with other neurotropic viruses.

KEYWORDS rabies virus, blood-brain barrier, permeability change, matrix metallopeptidase 8, inflammation

Rabies, caused by rabies virus (RABV), presents a public health threat to people living in undeveloped countries. RABV is a negative single-stranded RNA (ssRNA) virus and belongs to the *Rhabdoviridae* family. Analysis of recovered rabies patients revealed that the blood-brain barrier (BBB) plays an important role in protection against the virus (1–4). In the mouse model, wild-type (wt) RABV resulted in mild inflammation. However, extensive inflammation,

Editor Bryan R. G. Williams, Hudson Institute of Medical Research

Address correspondence to Ling Zhao, zling604@outlook.com.

The authors declare no conflict of interest.

Received 7 July 2022
Accepted 2 August 2022
Published 25 August 2022

apoptosis, and expression of innate immunity genes have been found in the central nervous system (CNS) of mice infected with lab-attenuated RABV (5). Moreover, BBB permeability is enhanced in mice infected with lab-attenuated RABV but not in mice infected with wt RABV (5, 6). Enhancing BBB permeability is important in RABV attenuation by allowing immune cells to enter the CNS and clear the virus (5, 7, 8). The enhancement of BBB permeability by administering lab-attenuated RABV, or immune-stimulating agents, cleared wt RABV from the CNS and prevented the development of rabies in mice (9–12). Therefore, BBB permeability has attracted much attention from researchers interested in rabies pathogenesis and treatment.

The BBB comprises endothelial cells, pericytes, and astrocytes and separates the circulating blood from the cerebrospinal fluid, protecting the CNS from circulating cells and various factors (13). The presence of specific tight junction (TJ) proteins seals the space between adjacent endothelial cells. The TJ complex comprises transmembrane TJ proteins (occludin and claudins) and cytosolic TJ proteins (zonula occludens). The occludins and claudins can interact with zonula occludens (ZO), cytoplasmic adaptor proteins, which link to apical actin filaments to form tight seals between adjacent cells (14, 15). One of the key mechanisms of BBB breakdown observed in both bacterial and viral infection is the reduction of TJ proteins (16). The degradation of occludin, claudin-5, and ZO-1 indicates BBB disruption (17).

Various neurological disorders, such as bacterial meningitis (18) and neurotropic virus infection, including human immunodeficiency virus (HIV) (19, 20), Japanese encephalitis virus (JEV) (21, 22), and West Nile virus (WNV) (23–25), can cause increased permeability of the BBB. In only a few cases, viral gene products are directly involved in BBB disruption; in the absence of such mechanisms, indirect effects of the virus on the immune system may be responsible for barrier disruption (16). The role of matrix metallopeptidases (MMPs) in BBB damage from neurological disorders has been implicated in several studies. Mouse adenovirus type 1 infection can enhance the activity of MMP2/9 (26). WNV increases the levels of MMPs, which degrade TJ proteins and enhance BBB permeability (23). JEV-infected astrocytes release vascular endothelial growth factor, IL-6, and MMP2/MMP9, leading to ZO-1 degradation and disruption of BBB integrity (27). MMP8 plays a crucial role in the cleavage of occludin and cell adhesion during bacterial meningitis (18).

Our previous studies have shown that the increased permeability of the BBB caused by RABV infection is not directly due to viral infection but rather is due to virus-induced cytokines (28). In recent years, exploration of BBB disruption during RABV infection has focused on chemokines and cytokines such as gamma interferon (IFN-γ), tumor necrosis factor alpha (TNF-α), interleukin 6 (IL-6), CCL2, CXCL10, and IL-17 (8, 29–37). However, the molecular mechanism leading to BBB permeability change and whether MMPs play a role in this process remain unknown. In the present study, we found that the enhancement of BBB permeability and the reduction of TJ proteins caused by lab-attenuated RABV are regulated mainly by MMP8. Furthermore, lab-attenuated RABV upregulated the expression of MMP8 via the nuclear factor κB (NF-κB) and mitogen-activated protein kinase (MAPK) pathways. This finding can help us understand the molecular mechanisms underlying BBB disruption caused by RABV and provide potential therapeutic targets for the clinical treatment of rabies.

RESULTS

Expression of MMP8 is upregulated in the mouse brain and neuronal cells after lab-attenuated RABV infection but not wild-type RABV infection. Since our previous studies have established the mouse model to compare infections with a lab-attenuated RABV strain, CVS-B2c (CVS), and a dog-derived RABV strain, DRV-Mexico (DRV) (38, 39), we used this model to investigate the role of the MMP family in the BBB permeability change during RABV infection. C57/BL6 mice were inoculated intracranially (i.c.) with 20 focus-forming units (FFU) of CVS or 200 FFU of DRV or were mock infected with the same volume of Dulbecco's modified Eagle's medium (DMEM). At 6 days postinfection (d.p.i.), the mice were euthanized with CO_2, and the mouse brains were collected and subjected to RNA isolation. Then the mRNA levels of MMPs, which have been indicated to impact BBB integrity (18, 40–43), were selected and then quantified by quantitative real-time PCR (qRT-PCR, or simply qPCR). The results showed that the mRNA levels of MMP3, MMP8, MMP9, and MMP12 were significantly upregulated at 6 d.p.i. during CVS infection, with MMP8 showing the most

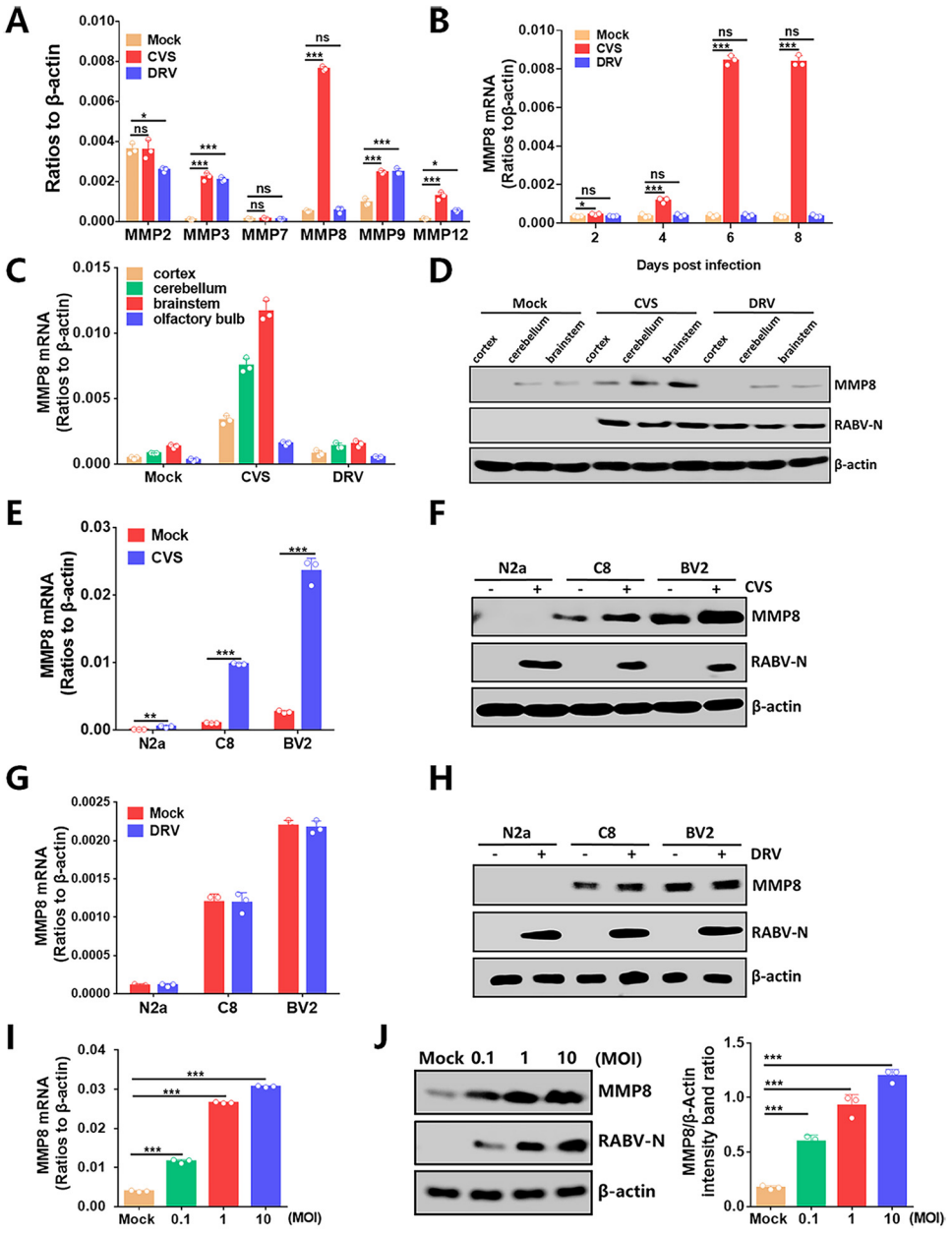

FIG 1 MMP8 expression is upregulated by lab-attenuated RABV infection in cells and mouse brains. C57BL/6 mice (n = 3) were intracerebrally (i.c.) inoculated with 20 FFU of RABV strain CVS-B2c (CVS), 200 FFU of DRV-Mexico (DRV), or the same volume of DMEM (mock). At 2, 4, and 6 d.p.i., mouse brains were harvested and used for further analysis. (A) At 6 d.p.i., total RNA was isolated from brain tissue and analyzed by qPCR for mRNA levels of MMP2, -3, -7, -8, -9, and -12. (B) At 2, 4, 6, and 8 d.p.i., total RNA from mouse brains was isolated, and the MMP8 mRNA level was analyzed by qPCR. (C) At 6 d.p.i., total RNA from different brain sections was isolated, and the MMP8 mRNA level was analyzed by qPCR. (D) At 6 d.p.i., the protein levels of MMP8 and RABV-N in the mouse cortex, cerebellum, and brain stem were assessed by Western blotting; β-actin was used as the control. (E) BV2, C8, and N2a cells were infected with CVS at an MOI of 1, and MMP8 mRNA levels were measured by qPCR at 48 h postinfection (h.p.i.). (F) MMP8 protein levels in BV2, C8, and N2a cells after CVS infection were measured by Western blotting. (G) BV2, C8, and N2a cells were infected with DRV at an MOI of 1, and MMP8 mRNA levels were measured using qPCR at 48 h.p.i. (H) MMP8 protein levels in BV2, C8, and N2a cells after DRV infection were measured by Western blotting. (I) BV2 cells were infected with CVS at the indicated MOIs, and MMP8 mRNA levels were measured using qPCR. (J) BV2 cells were infected with CVS at indicated MOIs, and MMP8 protein levels were assessed using Western blot. The gray value of MMP8 and β-actin was calculated using ImageJ software. Error bars represent SD (n = 3). Statistical differences between infected group and mock-infected group were determined using the Student t test. Western blot data are representative of those from at least two independent experiments. ns, not significant.

evident increase (Fig. 1A). We also found that only the mRNA levels of MMP8 and MMP7 were unaffected during DRV infection (Fig. 1A). Since our recent study confirmed that BBB permeability was significantly increased upon CVS infection, while the BBB was intact under DRV infection, we then focused on the effect of MMP8 on BBB permeability during CVS infection in the following study (28).

First, we examined MMP8 mRNA levels in mouse brains infected with CVS or DRV at different time points by qPCR. We found that MMP8 was induced in CVS-infected but not in DRV-infected mouse brains at 2, 4, 6, and 8 d.p.i. (Fig. 1B). Then, the mRNA level of MMP8 in different brain regions upon the infection of CVS at 6 d.p.i. was measured by qPCR, and the results showed that all four brain regions (olfactory bulb, cortex, cerebellum, and brain stem) had an increased MMP8 mRNA level under infection with CVS but not infection with DRV (Fig. 1C). We also observed that MMP8 is mainly distributed in the cerebellum and brain stem (Fig. 1C). Western blot analysis was also performed and confirmed that the protein level of MMP8 in different brain regions (cortex, cerebellum, and brain stem) was increased upon infection with CVS but not DRV (Fig. 1D).

To further confirm the above observations, N2a (neuron), C8 (astrocyte), and BV2 (microglia) cell lines were infected with CVS or DRV at a multiplicity of infection (MOI) of 1 and incubated for 48 h. Then total RNA was harvested, and mRNA levels of MMP8 were quantified using qPCR. The results showed that the MMP8 mRNA level was significantly upregulated post-CVS infection in these three cell lines (Fig. 1E), while the MMP8 mRNA level was unchanged under DRV infection in all three cell lines (Fig. 1G). Western blot analysis also confirmed that the MMP8 protein level was significantly upregulated under CVS infection in the C8 and BV2 cell lines (Fig. 1F) but not under DRV infection (Fig. 1H). It should be noted that the MMP8 protein level in N2a cells was too low to be measured by Western blotting. Since BV2 cells showed the most abundant MMP8 protein level, we further measured MMP8 expression level post-CVS infection at different MOIs (0.1, 1, and 10) in BV2 cells. Both qPCR and Western blot analysis showed that MMP8 was significantly upregulated upon CVS infection at the indicated MOIs (Fig. 1I and J). Altogether, these results demonstrate that infection with CVS could upregulate the expression of MMP8 both *in vivo* and *in vitro*.

MMP8 expression is regulated by inflammation via the NF-κB and MAPK pathways. MMP8 has been reported to have a tight association with the inflammatory response. Also, our previous research has confirmed that CVS infection could elicit a strong inflammatory response in the brain, so we wondered if the inflammation induced by CVS infection mediates MMP8 production (5, 44). We used CVS and DRV to infect mouse brains and quantified their inflammatory activation level by Western blotting. The results showed that CVS infection could elicit a strong inflammatory response in mouse brains, while DRV infection could not (Fig. 2A). Then, we used lipopolysaccharide (LPS) and IFN-γ (both classical inflammatory stimulants) to treat BV2 cells and found that both MMP8 mRNA and protein levels were upregulated (Fig. 2B and C).

Previous studies have found that two primary inflammatory pathways, the NF-κB and MAPK pathways, were activated by CVS infection (45). The signal transduction pathways mediated by the MAPK family, including extracellular signal-regulated kinases 1 and 2 (ERK1/2), c-Jun N-terminal kinase (JNK), and p38, contribute to the activation of transcription factors (46). To further investigate which inflammatory pathway was responsible for MMP8 production, different inhibitors against the NF-κB (QNZ), p38 (p38 MAPK inhibitor IV), ERK (ERK inhibitor), and JNK (JNK-IN-8) pathways were treated with CVS-infected BV2 cells. qPCR (Fig. 2D) and Western blot (Fig. 2E) results showed that all four pathways were associated with MMP8 production, but inhibition of a single pathway could not lead to the complete obliteration of MMP8 production compared with the mock-infected cells. Collectively, our results demonstrated that the NF-κB, p38, ERK, and JNK pathways are involved in MMP8 production during CVS infection.

Transcription factors c-Fos and p65 bind with the MMP8 promoter and regulate its activity. To further elucidate how MMP8 expression was regulated, we analyzed the promoter region of MMP8. An approximately 2.5-kb DNA fragment containing noncoding sequences upstream from the MMP8 transcriptional initiation site (TSS) was cloned for promoter mapping. Luciferase reporter genes with different lengths of the MMP8 putative promoter

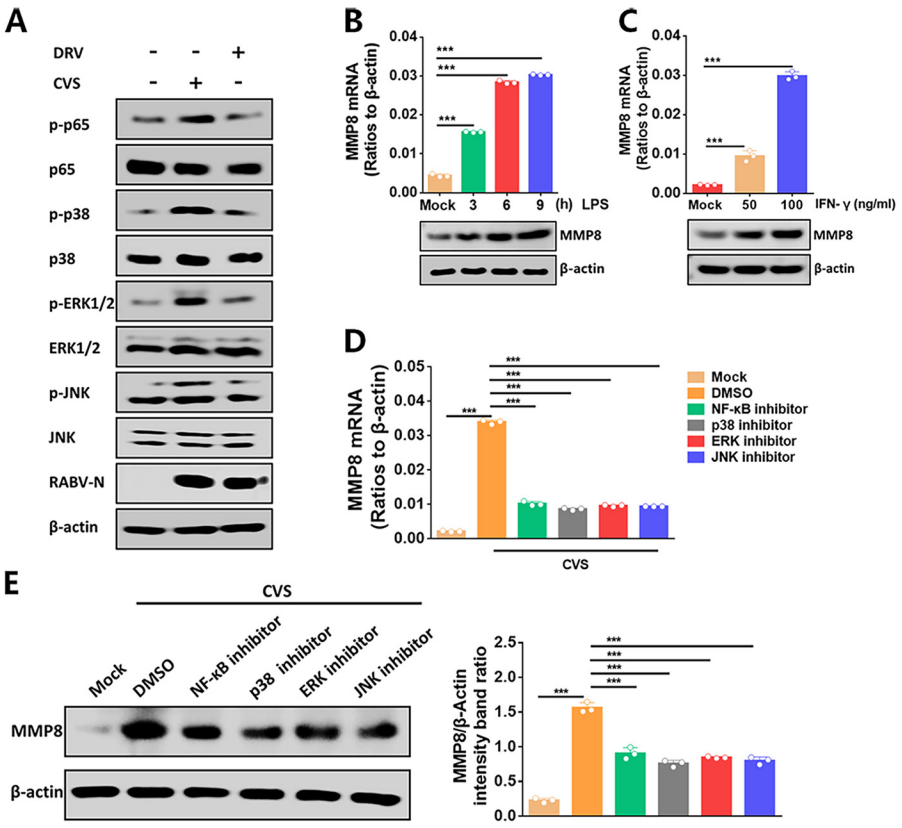

FIG 2 MMP8 expression is regulated via NF-κB and MAPK pathways. (A) C57BL/6 mice (n = 3) were i.c. inoculated with 20 FFU of CVS or 200 FFU of DRV. Mouse brains from each group at 6 d.p.i. were harvested. The expression and phosphorylation of the key molecules in the NF-κB and MAPK pathways in CVS- or DRV-infected mouse brains were measured by Western blotting. (B) BV2 cells were incubated with LPS (100 ng/mL) for the indicated periods. MMP8 mRNA and protein levels were measured by qPCR and Western blotting. (C) BV2 cells were incubated with IFN-γ at the indicated concentrations. MMP8 mRNA level and protein level were measured by qPCR and Western blotting. (D and E) BV2 cells were infected with RABV at an MOI of 1, and at different time points after RABV infection, the culture medium was replaced with specific inhibitors (p38 inhibitor, 1 μM, 24 h; NF-κB inhibitor, 5 μM, 24 h; JNK inhibitor, 0.5 μM, 12 h; ERK inhibitor, 5 μM, 24 h) or dimethyl sulfoxide (DMSO). (D) The mRNA levels of MMP8 were quantified by qPCR. (E) MMP8 protein levels were assessed using Western blotting. The gray value of MMP8 and β-actin was calculated using ImageJ software. Anti-MMP8 antibody, 500 ng/mL; anti-β-actin antibody, 500 ng/mL. Statistical analysis of comparisons between groups was carried out by the Student t test. The bar graph shows the means ± SD (n = 3). The Western blot data are representative of those from at least three independent experiments.

regions were constructed and transfected into N2a cells. The basal and CVS-induced promoter activities were then evaluated. As shown in Fig. 3A, the full-length reporter (TSS-2500) displayed high basal promoter activity and obvious RABV inducibility, which was decreased by three truncations of this full-length region, termed TSS-2000, TSS-1500, and TSS-1000. However, the reporter TSS-500 had a higher luciferase activity in both mock-infected N2a cells and RABV-infected N2a cells, comparable to that of the longest reporter TSS-2500, suggesting that TSS-500 possesses fully intact promoter activity.

Consequently, the TSS-500 reporter was an MMP8 promoter responsive to RABV infection and thus was chosen for further analysis. To further analyze whether inflammatory pathways play an important role in the regulation of MMP8 expression induced by RABV, specific inhibitors of signaling pathways were employed. The results demonstrated that all these four pathways were involved MMP8 promoter activation, but only inhibition of all the four pathways could completely abolish MMP8 promoter activity (Fig. 3B).

Bioinformatics analyses of the MMP8 promoter region (TSS-500) using PROMO and JASPAR software predicted several potential transcription factor-binding sites. The putative binding sequences for two potential transcription factors, AP-1 (c-Fos) and NF-κB (p65), were found within the MMP8 promoter. To determine if these predicted transcription factors were

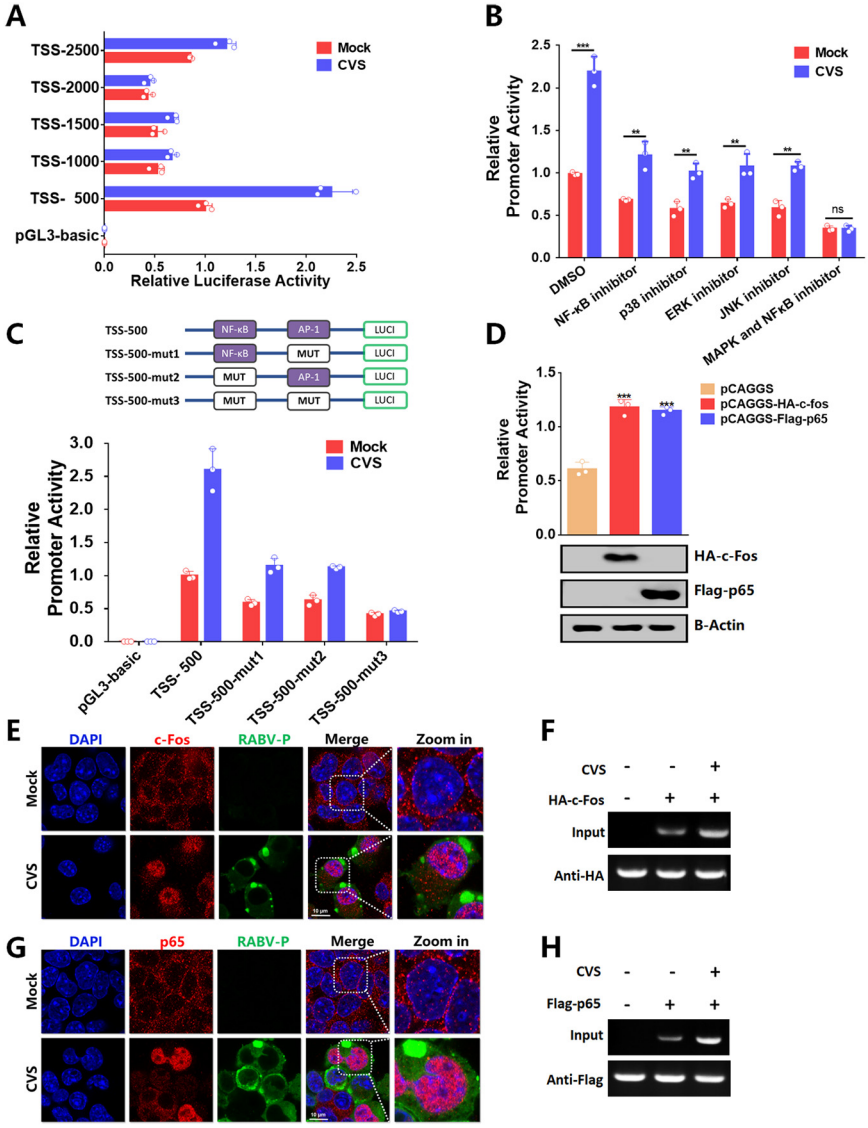

FIG 3 c-Fos and p65 elements regulate MMP8 promoter activity. (A) N2a cells were transfected with MMP8 promoter reporter plasmids (TSS-500, TSS-1000, TSS-1500, TSS-2000, and TSS-2500) for 24 h. Then cells were either infected with CVS at an MOI of 0.1 or left uninfected, and the luciferase activities were measured after a further 24 h of infection. (B) N2a cells were transfected with the MMP8 promoter reporter plasmid: TSS-500. At 24 h posttransfection, cells were infected with CVS at an MOI of 0.1, and at different time points after RABV infection, the culture medium was replaced with different signaling pathway-specific inhibitors (p38 inhibitor, 1 μM, 24 h; NF-κB inhibitor, 5 μM, 24 h; JNK inhibitor, 0.5 μM, 12 h; ERK inhibitor, 5 μM, 24 h; MAPK and NF-κB inhibitor, 20 μM, 24 h) or DMSO. After 24 h infection, MMP8 promoter luciferase activity was measured. (C) Schematic representation of point mutations in the wild-type promoter reporter (TSS-500). N2a cells were transfected with the MMP8 promoter reporters (TSS-500 and its mutants). At 24 h posttransfection, cells were either left uninfected or infected with CVS at an MOI of 0.1, and luciferase activity was measured after 24 h of infection. (D) N2a cells were cotransfected with MMP8 promoter reporter (TSS-500) plasmid or HA-c-Fos- or Flag-p65-expressing plasmid for 24 h. Dual-luciferase assays measured the MMP8 promoter activities. The expression of HA-c-Fos and Flag-p65 was determined by Western blotting. (E and G) N2a cells were mock infected (top) or infected with CVS (bottom) at an MOI of 0.1. (E) At 36 h.p.i., the cells were fixed, and c-Fos proteins (left), RABV-N (middle), and cell nuclei (right) were stained as described in the text. (G) At 36 h.p.i., the cells were fixed, and p65 proteins (left), RABV-N (middle), and cell nuclei (right) were stained as described in the text. (F and H) N2a cells were transfected with plasmids encoding HA-c-Fos or Flag-p65 for 24 h and then infected with CVS at an MOI of 0.1. Fixed chromatin from N2a cells was prepared and immunoprecipitated by anti-HA or anti-Flag antibodies. ChIP primers were designed to amplify the region containing respectively c-FOS and p65 binding site in the MMP8 promoter. PCR products were separated by acrylamide gel electrophoresis. Statistical analysis of comparisons between groups was carried out by the Student *t* test. The bar graph shows the means ± SD (n = 3). Scale bar = 10 μm. Western blot data are representative of those from at least two independent experiments.

responsive to MMP8 transcription, a series of mutated promoter constructs, including full-length (TSS-500-WT), mutation AP-1 (TSS-500-mut1, AAGTACTTTCC to AACTTCAATGG), mutation NF-κB (TSS-500-mut2, ATGACTCC to AATTCGGC), and mutations AP-1 and NF-κB (TSS-500-mut3, AAGTACTTTCC to AACTTCAATGG and ATGACTCC to AATTCGGC) were generated and tested for their promoter activity under CVS infection (Fig. 3C). The results showed that in comparison with the TSS-500-WT, mutation of AP-1 or NF-κB binding sites exhibited significantly less response to CVS infection, while mutation of both two binding sites could completely abrogate CVS-mediated induction of MMP8 promoter activity (Fig. 3C), suggesting that activation of the MMP8 promoter by CVS infection requires both AP-1 and NF-κB elements.

Next, we constructed the expression plasmids pCAGGS-Flag-p65 (named Flag-p65) and pCAGGS-HA-c-Fos (named HA-c-Fos) and confirmed that expression of AP-1 or NF-κB could activate MMP8 promoter activity (Fig. 3D). Since transcription factors need to transport into the cell nucleus and bind to corresponding DNA fragments to exert their function, we tested whether CVS infection could lead to the nuclear translocalization of c-Fos and p65. Confocal microscopy analysis showed that c-Fos and p65 were translocated into the nucleus post-CVS infection (Fig. 3E and G). We further used chromatin immunoprecipitation assay (ChIP) and confirmed that c-Fos and p65 could bind to the promoter of MMP8 after CVS infection (Fig. 3F and H). Altogether, these results demonstrate that MMP8 promoter activity is regulated by transcription factors c-Fos and p65.

Growth kinetics and pathogenicity of rRABV expressing MMP8 *in vitro* and *in vivo*. To investigate the effect of MMP8 on RABV replication and pathogenicity, we constructed and rescued a recombinant RABV (rRABV) expressing murine MMP8, named rRABV-MMP8 (Fig. 4A). The success of rescuing rRABV-MMP8 was confirmed by immunofluorescence assay (IFA), with rRABV being a control (Fig. 4B). Using Western blot analysis, we showed that MMP8 was highly expressed in N2a cells infected with rRABV-MMP8 but not rRABV (Fig. 4C). N2a and BSR cells were infected with rRABV or rRABV-MMP8to test whether the expression of MMP8 could affect RABV replication. The growth dynamics demonstrated that rRABV-MMP8 replicated as efficiently as the parent virus rRABV in these cell lines (Fig. 4D and E).

To further assess the impact of MMP8 on the pathogenesis of RABV *in vivo*, we inoculated mice intracranially with rRABV and rRABV-MMP8 (20 FFU/mouse). The survival ratios were monitored daily. The results showed that the survival ratios were comparable between rRABV-infected and rRABV-MMP8-infected mice (Fig. 4F). Next, we analyzed the RABV-N mRNA level in RABV-infected mouse brains at 2, 4, and 6 d.p.i. qPCR results demonstrated that the viral load in rRABV-MMP8-infected mouse brains was not different from that in rRABV-infected mouse brains (Fig. 4G). Altogether, these results demonstrate that the pathogenicity of rRABV-MMP8 is similar to that of rRABV after intracranial infection.

MMP8 expression increases BBB permeability by degrading tight junction proteins during RABV infection *in vitro* and *in vivo*. To examine the effect of MMP8 on BBB permeability *in vivo*, we administered sodium fluorescein (NaF), a dye with a molecular weight of 41.99 Da and which is normally shielded by the BBB, into the mice via the intraperitoneal (i.p.) route at 2, 4, and 6 d.p.i. The results showed significantly higher levels of NaF in the whole brains of rRABV-MMP8-infected mice than in the rRABV-infected mouse brains at 2 and 4 d.p.i., while the NaF levels of the two groups were similar at 6 d.p.i. (Fig. 5A). We also collected the brains of mock-, rRABV-, and rRABV-MMP8-infected mice at 4 d.p.i. Western blotting was performed to measure the protein levels of the tight junction proteins ZO-1, occludin, and claudin-5. These results showed that all these three proteins were significantly degraded in rRABV-MMP8-infected mouse brains compared with the brains from the other two groups (Fig. 5B).

To evaluate the effect of MMP8 on BBB permeability in a Transwell model. Mock-, rRABV-, and rRABV-MMP8-infected mouse brains were collected and homogenized at 4 d.p.i. The supernatant from each group was collected for further experiments. The Transwell model results showed the permeability of dextran 10000 in bEnd.3 cells (mouse brain-derived endothelial cells) treated with the supernatant from rRABV-MMP8-infected mouse brains were higher than from rRABV-infected mouse brains (Fig. 5C). Next, the supernatant from each group was cultured with bEnd.3 cells to test its ability to degrade tight junction proteins ZO-1, occludin, and claudin-5. Both Western blot and IFA analyses showed that these three proteins were

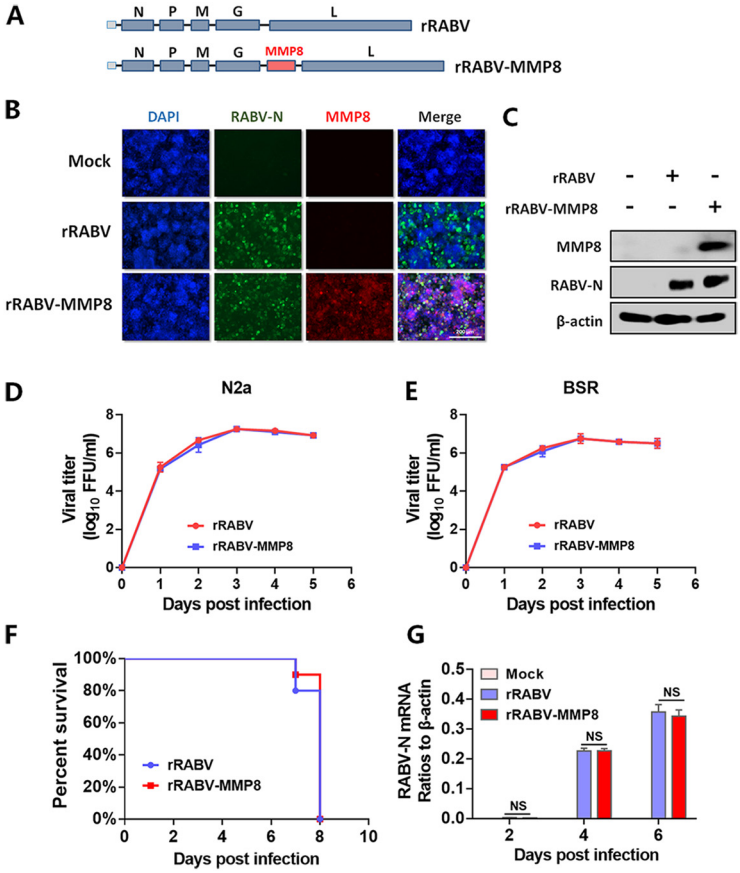

FIG 4 Effect of MMP8 expression on RABV replication and viral pathogenicity. (A) Schematic diagram of the construction of rRABV and rRABV-MMP8. (B) N2a cells were infected with rRABV or rRABV-MMP8 at an MOI of 0.1. At 36 h.p.i., the cells were fixed and stained to detect RABV-N and MMP8. (C) N2a cells were infected with rRABV or rRABV-MMP8 at an MOI of 0.1. At 36 h.p.i., cells were harvested, and the expression levels of RABV-N and MMP8 were detected by Western blotting. (D and E) N2a (D) and BSR cells (E) were infected with rRABV or rRABV-MMP8 at an MOI of 0.01 for the indicated times, and the supernatants were harvested for virus titration. (F) Female C57BL/6 mice (n = 10) were i.c. infected with 20 FFU of rRABV or rRABV-MMP8. The survival ratio was monitored daily (means ± SD; the survival ratio was analyzed by log rank test). (G) The mRNA levels of RABV-N in the whole brain were analyzed using qPCR at 2, 4, and 6 d.p.i. Statistical analysis of comparisons between groups was carried out by the Student t test. The bar graph shows the means ± SD. Scale bar = 200 μm. Western blot data are representative of those from at least two independent experiments. NS, not significant.

significantly degraded in bEnd.3 cells treated with the supernatant from rRABV-MMP8-infected mouse brains compared with mock- or rRABV-infected mouse brains (Fig. 5D and E). Altogether, these results indicate that MMP8 can degrade tight junction proteins and thus enhance BBB permeability.

MMP8 inhibitor prevents the degradation of tight junction proteins during RABV infection *in vitro* and *in vivo*. To further investigate the effect of MMP8 on the degradation of tight junction proteins *in vitro* and *in vivo*, the selective MMP8 inhibitor (MMP-8 inhibitor 1) was introduced to treat bEnd.3 cells along with the supernatant from rRABV-infected mouse brains. The results from Western blotting, the Transwell model, and immunofluorescence assay demonstrated that the degradation of ZO-1, occludin, and claudin-5 was inhibited upon treatment with the MMP8 inhibitor (Fig. 6A to C). To further verify the role of MMP8 on the degradation of tight junction proteins, we treated bEnd.3 cells with MMP8 protein. Western blotting and Transwell model results both confirmed that ZO-1, occludin, and claudin-5 had degraded after the treatment of MMP8 protein (Fig. 6D and E). Altogether, these results confirm that MMP8 is indispensable in degrading tight conjunct proteins under RABV infection *in vitro*.

To confirm this observation *in vivo*, we treated CVS-infected mice i.p. with MMP8

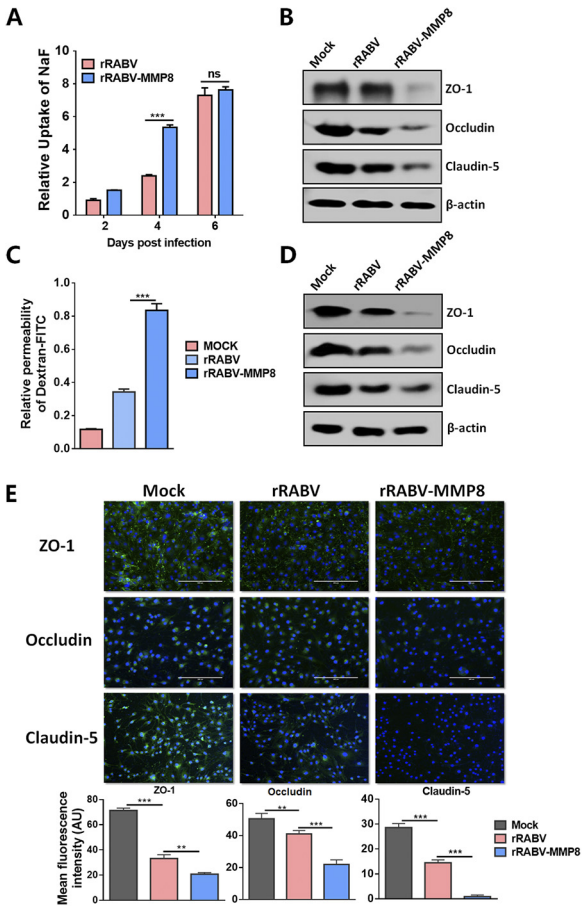

FIG 5 MMP8 expression enhances BBB permeability during RABV infection. C57BL/6 mice (n = 3) were i.c. inoculated with 20 FFU of rRABV or rRABV-MMP8. (A) At 2, 4, and 6 d.p.i., mice were injected intraperitoneally with 100 μL of NaF (100 mg/mL), and the BBB integrity was calculated based on NaF uptake in the brains. (B) At 4 d.p.i., mouse brains were harvested and used for further analysis. In mouse brains, protein levels of occludin, claudin-5, and ZO-1 were measured by Western blotting, and β-actin was included as a control. (C) At 4 d.p.i., mouse brains were harvested, homogenized, and centrifuged, and then the supernatants were harvested and treated with UV light for 30 min to eliminate live viruses. bEnd.3 cells in a Transwell model were treated with the supernatants, and the transendothelial permeability assay was performed to evaluate the integrity of bEnd.3 cells. (D and E) bEnd.3 cells were treated with supernatants for 48 h and then harvested to measure the occludin, claudin-5, and ZO-1 levels using Western blotting (D) and immunofluorescence (E). The mean fluorescence intensity of occludin, claudin-5, and ZO-1 in the respective groups was calculated using ImageJ software. Statistical analysis of comparisons between groups was carried out by the Student t test. The data are presented as means ± SD (n = 3). Scale bar = 200 μm. Western blot data are representative of those from at least two independent experiments.

selective inhibitor as previously described (47). Then we administered NaF into the mice via the i.p. route at 6 d.p.i. Significantly higher levels of NaF in the whole brains of CVS-infected mice were observed than in the brains of CVS-infected mice treated with the MMP8 inhibitor (Fig. 6F). Western blot analysis further confirmed that the degradation of ZO-1, occludin, and claudin-5 inside CVS-infected mouse brains was inhibited upon the treatment of the MMP8 inhibitor (Fig. 6G). It should be noted that the MMP8 inhibitor could not fully restore the BBB permeability of CVS-infected brains compared with that of mock-infected mouse brains (Fig. 6F), suggesting that MMP8 is not the only determinant affecting opening of the BBB during CVS infection.

MMP8 expression upregulates production of inflammatory cytokines and infiltration of inflammatory cells in the brain post-RABV infection. Increased BBB permeability will cause extensive inflammation in the brain. To confirm whether increased inflammation-related cytokines and chemokines were transcribed in rRABV-MMP8-infected mouse brains compared to rRABV-infected mouse brains, we quantified several inflammatory genes, including those for TNF-α, CCL5, IL-6, and CXCL10, by qPCR.

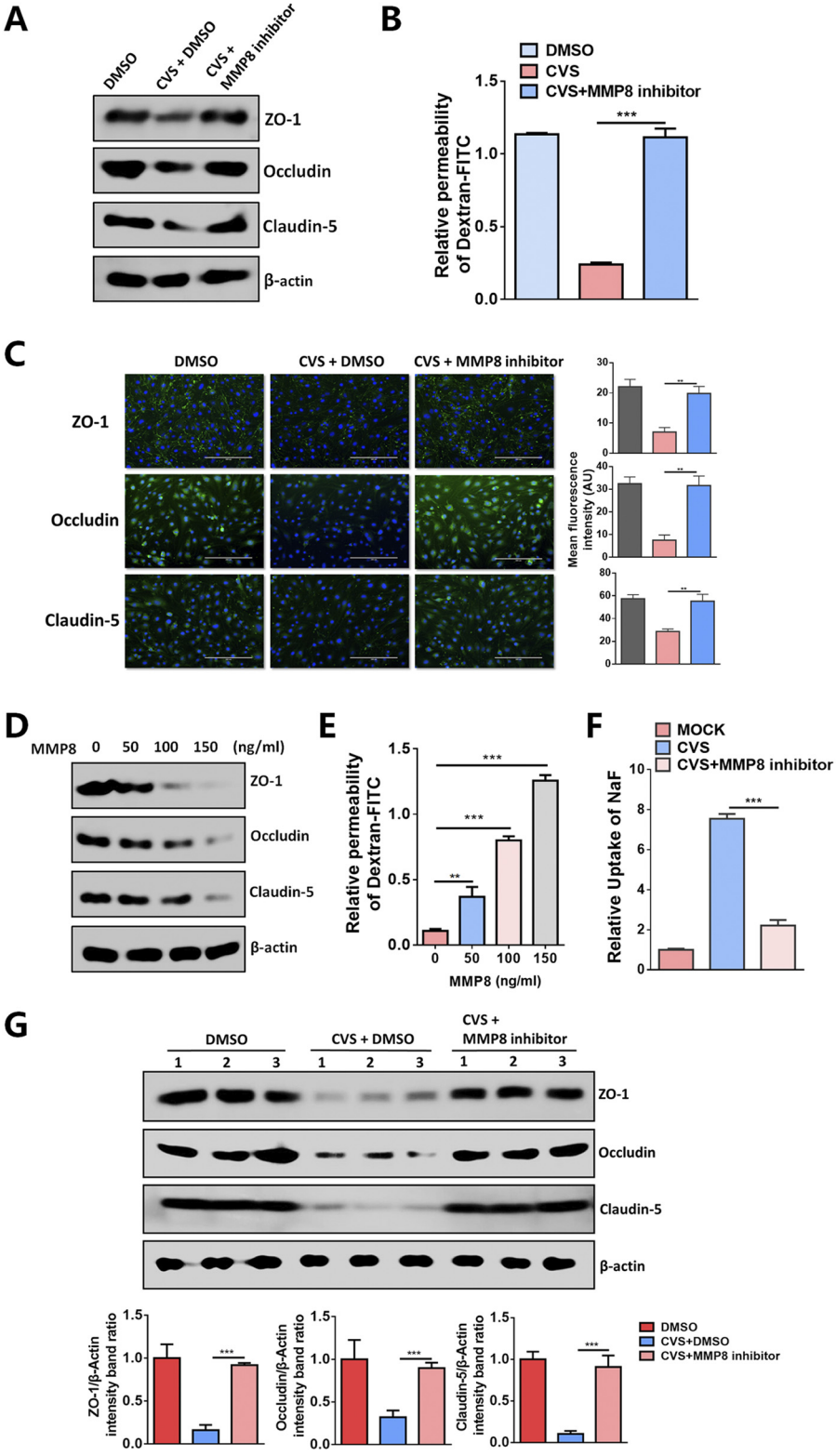

FIG 6 MMP8 degrades TJ proteins during RABV infection. C57BL/6 mice (n = 3) were i.c. inoculated with 20 FFU of rRABV or mock infected with DMEM at the same volume. At 6 d.p.i., mouse brains were harvested and used for further analysis. (A and C) bEnd.3 cells were treated with supernatants (prepared as for Fig. 5C) in the presence of MMP8 specific inhibitors (10 μM) or DMSO for 48 h and then harvested to measure the occludin, claudin-5, and ZO-1 levels by Western blotting (A) and immunofluorescence (C). (B) bEnd.3 cells in a Transwell model were treated with supernatants, and a transendothelial permeability assay was performed to evaluate the integrity of bEnd.3 cells. (D) The occludin, claudin-5, and ZO-1 expression levels in bEnd.3 cells

(Continued on next page)

The results showed that the transcription of these inflammatory cytokines/chemokines in rRABV-MMP8-infected mouse brains was significantly higher than that in rRABV-infected mouse brains at 4 d.p.i., while these differences disappeared at 6 d.p.i. (Fig. 7A to D). Furthermore, Western blot analysis showed no differences in the activation levels of the NF-κB and MAPK pathways in mouse brains infected with rRABV or rRABV-MMP8 at 6 d.p.i. (Fig. 7E), which could partially explain why the pathogenicity of rRABV-MMP8 is similar to that of rRABV after i.c. infection.

Increased BBB permeability also facilitates the infiltration of peripheral immune cells into the CNS (48). To explore whether there were more peripheral immune cells in rRABV-MMP8-infected mouse brains than in rRABV-infected mouse brains in early stages of infection, we homogenized the mouse brains at 4 d.p.i., isolated the leukocytes, and analyzed them by flow cytometry. Several cell types infiltrated into rRABV-MMP8-infected mouse brains were observed, including neutrophils ($CD45^{hi}$ $Ly6G^{+}$), $CD4^{+}$ T cells ($CD45^{+}$ $CD4^{+}$), $CD8^{+}$ T cells ($CD45^{+}$ $CD8^{+}$), B cells ($CD11c^{-}$ $CD45^{+}$ $B220^{+}$), and macrophages ($CD45^{hi}$ $CD11b^{+}$) (Fig. 7F to J). When the rRABV and rRABV-MMP8 groups were compared, significantly more macrophages, neutrophils, and $CD4^{+}$ T, $CD8^{+}$ T, and B cells were found in the brains from rRABV-MMP8-infected mice than in those from rRABV-infected mice, indicating that MMP8 could facilitate infiltration of macrophages, neutrophils, T cells, and B cells into mouse brains post-RABV infection.

DISCUSSION

This study demonstrates that MMP8 regulates the reduction of TJ protein expression and the enhancement of BBB permeability during RABV infection. Our focus on infection with different RABV strains further uncovered that lab-attenuated RABV can upregulate MMP8 by activating the MAPK and NF-κB pathways, whereas wt RABV does not. wt RABV shows little or no effect on inflammatory response activation in the brain and thus failed to induce the expression of MMP8, resulting in the close of BBB (Fig. 8).

While the expression of MMP8 in the brains of mice infected with lab-attenuated RABV was significantly increased, this phenomenon did not present in mice infected with wt RABV. We found that MMP8 was mainly derived from activated microglia and astrocytes. Previous studies reported that the expression of MMP2/9 was regulated by the MAPK and NF-κB pathways (49–51), and the expression of MMP8 was significantly increased in LPS-activated microglia (44). Thus, we speculated that MMP8 might be regulated by the same or other inflammatory pathways. Consistent with this hypothesis, previous studies have found that lab-attenuated RABV but not wt RABV activates innate immunity and induces an inflammatory response (5, 52, 53). Although the detailed mechanisms are not fully understood, at least we have found that double-stranded RNA (dsRNA) and ssRNA produced by the lab-attenuated RABV during viral replication can activate the mitochondrial antiviral signaling protein (MAVS) and Toll-like receptor (TLR7) signaling pathways and thus induce an inflammatory response (48, 52).

FIG 6 Legend (Continued)
were determined by Western blotting after treatment with MMP8 recombinant protein at the indicated concentrations. (E) bEnd.3 cells in a Transwell model were treated with MMP8 recombinant protein at the indicated concentrations, and a transendothelial permeability assay was performed to evaluate the integrity of bEnd.3 cells. (F and G) Two groups of C57BL/6 mice (n = 3) were i.c. inoculated with 20 FFU of CVS. One group of C57BL/6 mice (n = 3) were i.c. inoculated with the same volume of DMEM. MMP8 selective inhibitor was dissolved in 1% DMSO in PBS to a final concentration of 0.01 mg/mL. The CVS-infected mice received a 1-mg/kg (of body weight) dose of inhibitor or the same volume of a vehicle (1% DMSO in PBS) at 2 and 4 d.p.i. At 6 d.p.i., mice were injected intraperitoneally with 100 μL of NaF (100 mg/mL), and the BBB integrity was calculated based on NaF uptake in the brains (F). The infected mouse brains at 6 d.p.i. were collected, and the occludin, claudin-5, and ZO-1 expression levels were determined by Western blotting (G). The mean fluorescence intensity of occludin, claudin-5, and ZO-1 in the respective groups was calculated using ImageJ software. Statistical differences between virus-infected cells and mock-infected cells were determined using the Student t test. The data are presented as means $\pm$ SD (n = 3). Scale bar = 200 μm. Western blot data are representative of those from at least two independent experiments.

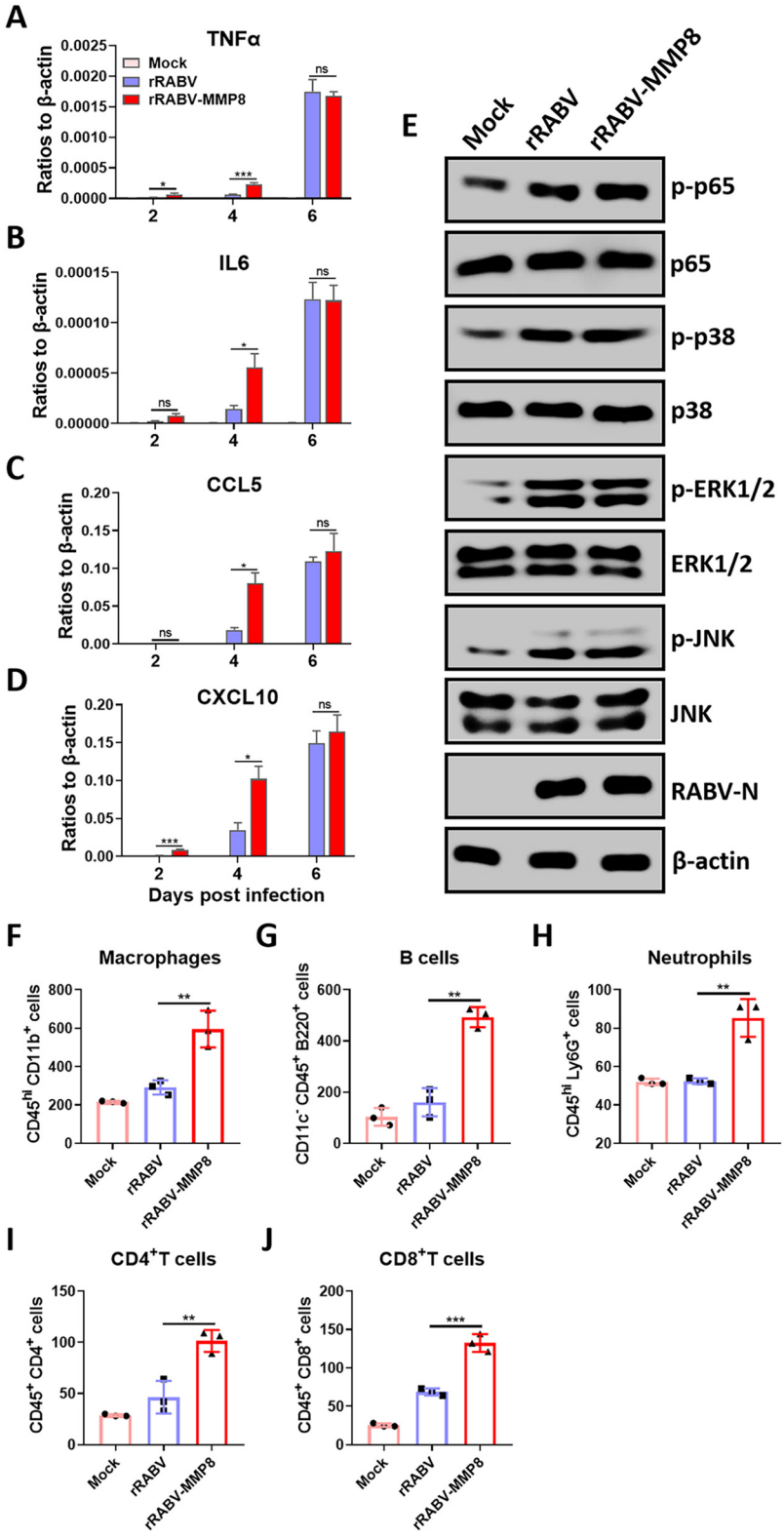

FIG 7 MMP8 expression increases the cytokine production and infiltration of inflammatory cells into the CNS. C57BL/6 mice (n = 3) were i.c. inoculated with 20 FFU of rRABV or rRABV-MMP8 or the same volume of DMEM (mock). (A to D) At 2, 4, 6 d.p.i., brains were harvested, and the transcription levels of TNF-α (A), IL-6 (B), CCL5 (C), and CXCL10 (D) were analyzed by qPCR. (E) At 6 d.p.i., brains were harvested, and the expression and phosphorylation of the key molecules in the NF-κB and MAPK pathways were measured by Western blotting. (F to J) At 4 d.p.i., mouse brains were homogenized, and leukocytes were isolated for

(Continued on next page)

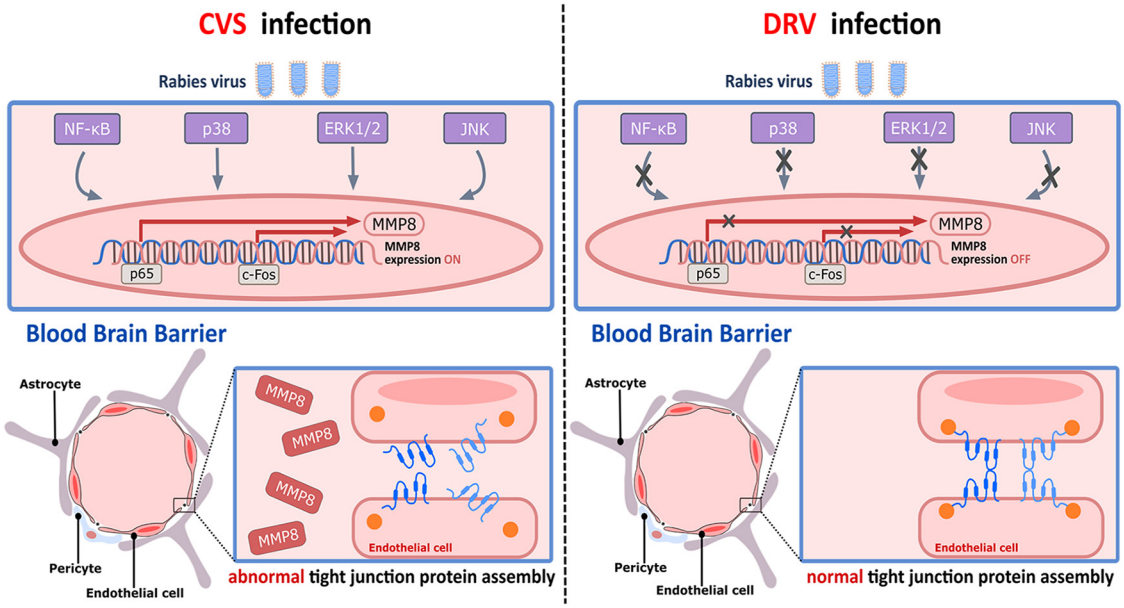

FIG 8 Schematic representation of mechanisms for MMP8 to regulate BBB permeability change during RABV infection. Lab-attenuated RABV rather than wt RABV can cause the activation of immune cells and lead to the activation of inflammation via the NF-κB and MAPK pathways. Translocated NF-κB (p65) and AP-1 (c-Fos) bind to the MMP8 promoter region and enhance its transcription, resulting in the upregulation of MMP8 production. Secreted MMP8 leads to the degradation of tight junction proteins, including occludin, claudin-5, and ZO-1, between the endothelial cells, resulting in disruption of the BBB.

The BBB is a physical and physiological barrier that controls the entry of cells and molecules into the CNS (13). The change of BBB is a pathological hallmark in neurological diseases (54). However, opening of the BBB facilitates the clearance of RABV from the CNS and the prevention of rabies (6). In the mouse model with RABV infection, lab-attenuated RABV can enhance BBB permeability. In contrast, wt RABV cannot enhance BBB permeability (5, 6). Our previous studies showed that chemokine and cytokines induced by lab-attenuated RABV were associated with BBB disruption (28). Here, we found that lab-attenuated but not wt RABV infection could induce the production of MMP8 via the MAPK and NF-κB pathways, which is consistent with the previous studies (5, 45). In addition, the specific inhibitors of the MAPK and NF-κB pathways can reduce the expression of MMP8 in RABV-activated microglia. We also found that lab-attenuated RABV could promote the binding of AP-1 and NF-κB transcription factors to the MMP8 promoter. Therefore, we confirmed that RABV regulates MMP8 expression through the MAPK- and NF-κB-dependent pathways. Consequently, the differences between lab-attenuated RABV and wt RABV in stimulating inflammatory pathways can account for their contrasting results in MMP8 regulation.

MMPs are key mediators responsible for altering BBB dysfunction (55–57). These zinc-dependent enzymes with proteolytic activity can regulate the BBB by cleaving tight junction proteins. The degradation of TJ proteins by MMP2 and MMP9 is an important mechanism of blood-brain barrier breakdown in neuromyelitis optica and HIV infection (58–60). MMP8 plays a key role in the degradation of occludin during meningococcal infection, leading to disruption of the BBB (18). In spinal cord injury, MMP8 is associated with the degradation of occludin and ZO-1 and the blood-spinal cord barrier (61). In addition, MMP8 inhibition blocked middle cerebral artery occlusion/reperfusion-induced downregulation of claudin-5 (62). Given this information, we can infer that MMP8 may facilitate opening of the BBB during RABV infection.

FIG 7 Legend (Continued)
analysis of macrophages ($CD45^{hi}$ $CD11b^{+}$), B cells ($CD11c^{-}$ $CD45^{+}$ $B220^{+}$), neutrophils ($CD45^{hi}$ $Ly6G^{+}$), $CD4^{+}$ T cells ($CD45^{+}$ $CD4^{+}$), and $CD8^{+}$ T cells ($CD45^{+}$ $CD8^{+}$). A total of 20,000 events were acquired for cytometry data collection. Statistical analysis of comparisons between groups was carried out by the Student *t* test. The data are presented as means ± SD ($n = 3$).

To balance the virus load of MMP8-expressing recombinant RABV (rRABV-MMP8) and the parental virus (rRABV) in the brain, we infected the mice via the intracranial route. We found that rRABV-MMP8-infected mice had higher BBB permeability, more inflammatory cell infiltration, and higher expression of inflammatory factors at 2 and 4 d.p.i. than rRABV-infected mice. However, these phenotypes between these two groups were similar at 6 d.p.i., indicating that overexpressed MMP8 played a role in BBB opening early post-RABV infection. Furthermore, the viral load in rRABV-MMP8-infected mouse brains at 6 d.p.i. was no different from that in rRABV-infected mouse brains. These findings could account for the similarity in pathogenicity of rRABV-MMP8 and rRABV after i.c. infection. Additionally, we evaluated the pathogenicity of rRABV-MMP8 and rRABV by intramuscular (i.m.) inoculation into mouse hind legs. We found that the survival ratio of the rRABV-MMP8-inoculated mice was significantly higher than that in the rRABV-inoculated mice. Consistent with the previous studies (29), these results demonstrate that opening of the BBB is beneficial for the clearance of RABV in the brain. However, after i.m. infection, these two types of viruses replicated in different viral loads in mouse brains, making it difficult to compare opening of the BBB by balancing the viral load in the brains.

Our previous study revealed that lab-attenuated RABV infection could cause the degradation of occludin, claudin-5, and ZO-1 leading to the disruption of the BBB (28). The present results showed that the degradation of these three proteins in bEnd.3 cells treated with supernatant from rRABV-MMP8-infected mouse brains was more significant than that in cells treated with supernatant from rRABV-infected mouse brains. *In vitro*, incubation of bEnd.3 cells with MMP8 recombinant protein resulted in the degradation of occludin, claudin-5, and ZO-1. Similarly, in the Transwell model, the use of MMP8 recombinant protein can cause an increase in barrier permeability. Importantly, MMP8-specific inhibitors restored the disruption of TJ proteins and barriers caused by brain extracts from lab-attenuated RABV-infected mice.

Other researchers have suggested that a key factor in opening of the BBB by RABV infection is the production of IFN-γ by CD4-positive T cells entering from the periphery, which can cause a cytokine storm through a peroxynitrite ($ONOO^-$)-dependent pathway leading to opening of the BBB (8, 29–33). We did observe a significant increase in CD4-positive T cells in the brains of rRABV-MMP8-infected mice at 4 d.p.i. in our study (Fig. 7I) and a significant upregulation of MMP8 when stimulating BV2 cells with IFN-γ *in vitro*. Interestingly, we also found a significant decrease but not a complete reversion in opening of the BBB after using MMP8 inhibitors in mice (Fig. 6F), indicating that the inactivation of MMP8 cannot completely prevent opening of the BBB during RABV infection. Taken together, our results show that MMP8 plays an important role in modulating opening of the BBB.

In summary, our study reveals that MMP8 can modulate BBB permeability change during RABV infection. More importantly, understanding that the MMP8 is regulated by the transcriptional factors NF-κB and AP-1 will aid researchers in developing effective therapies against RABV and other neurotropic viruses that cause encephalitis.

MATERIALS AND METHODS

Cells, viruses, antibodies, inhibitors, and mice. N2a (mouse neuroblastoma), BV2 (mouse microglioma), C8 (mouse astrocytoma), BSR (cloned from BHK-21 [baby hamster kidney-21] cells), and bEnd.3 (brain-derived endothelial cells) cells were cultured in Dulbecco's modified Eagle's medium (DMEM; Thermo Fisher, USA) supplemented with 10% fetal bovine serum (FBS; Thermo Fisher). RABV strain CVS-B2c (CVS) (originated from CVS-24 virus by passaging in BHK-21 cells) and wt RABV strain DRV-Mexico (DRV) were stored in our laboratory. Monoclonal antibodies (MAb) against Flag tag, hemagglutinin (HA) tag, and β-actin were purchased from Medical & Biological Laboratories (MBL; Nagoya, Japan). MAb against RABV-N protein were prepared by our laboratory. Polyclonal antibodies (pAb) against MMP8, c-Fos, occludin, claudin-5, and ZO-1 were purchased from ABclonal Technology (Wuhan, China). Antibodies against p-p65 (S536, no. 3033), p65 (no. 8242), p-p38 (T180/Y204, no. 4511), p38 (no. 9212), p-ERK1/2 (T202/Y204, no. 4370), ERK1/2 (no. 4695), p-JNK (T183/Y185, no. 9251), and JNK (no. 9252) were purchased from Cell Signaling Technology (CST; MA, USA).

The JNK inhibitor (no. GC13841), the NF-κB inhibitor (no. GC11751), the p38 inhibitor (no. GC18602), the ERK inhibitor (no. GC43624), the MAPK and NF-κB inhibitor (no. GC35411), and the MMP8 inhibitor (no. GC18616) were all purchased from Glpbio (Montclair, CA, USA). All the mouse experiments were performed following the recommendations in the Guide for the Care and Use of Laboratory Animals of the Ministry of Science and Technology of China and were approved by the Scientific Ethics Committee of Huazhong Agricultural University (permit no. HZAUMO-2017-055).

TABLE 1 Primers used for qPCR

Primer	Sequence (5′–3′)
MMP8-F	CCAAGGAGTGTCCAAGCCAT
MMP8-R	CCTGCAGGAAAACTGCATCG
MMP2-F	GCACATCCTATGACAGCTGC
MMP2-R	TTTGTTGCCCAGGAAAGTGA
MMP9-F	GAGACTCTACACCCAGGACG
MMP9-R	GAAAGTGAAGGGGAAGACGC
MMP3-F	TTAAAGACAGGCACTTTTGGC
MMP3-R	CCCTCGTATAGCCCAGAACT
MMP7-F	CTGCCACTGTCCCAGGAAG
MMP7-R	GGGAGAGTTTTCCAGTCATGG
MMP12-F	CTGCTCCCATGAATGACAGTG
MMP12-R	AGTTGCTTCTAGCCCAAAGAAC
IL6-F	ACAGAAGGAGTGGCTAAGGA
IL6-R	CGCACTAGGTTTGCCGAGTA
TNFα-F	TCACTGGAGCCTCGAATGTC
TNFα-R	GTGAGGAAGGCTGTGCATTG
CXCL10-F	CCAAGTGCTGCCGTCATTTTC
CXCL10-R	GGCTCGCAGGGATGATTTCAA
β-actin-F	GGCTGTATTCCCCTCCATCG
β-actin-R	CCAGTTGGTAACAATGCCATGT
RABV-N-F	ACACCGCAACTACAAGACA
RABV-N-R	ATGGTACTCCAGTTGGCACA
CCL5-F	GCTGCTTTGCCTACCTCTCC
CCL5-R	TCGAGTGACAAACACGACTGC

Virus titration. BSR and N2a cells were infected with rRABV or rRABV-MMP8 at a multiplicity of infection (MOI) of 0.01 for 1 h at 37°C. The cells were then washed with phosphate-buffered saline (PBS) three times and cultured in a cell incubator at 37°C. The supernatants were collected at 1, 2, 3, 4, and 5 d.p.i. The procedure applied for RABV titration was determined by direct immunofluorescence assay as described previously (63).

Construction and rescue of recombinant RABV. The recombinant viruses were constructed and rescued as described previously (63, 64). Briefly, the murine MMP8 gene was inserted into the genome of rRABV (cloned from strain CVS) strain between the G and L genes by replacing the pseudogene. The plasmid containing the full-length viral genome and the helper plasmids expressing the N, P, G, and L proteins was transfected into N2a cells using Lipofectamine 3000 (Thermo Fisher, USA) to rescue viruses, and the recombinant viruses were harvested at 5 d.p.i. The recombinant viruses were propagated and titrated on BSR cells.

Mouse infection. Female C57BL/6 mice (6 weeks old) were inoculated intracranially (i.c.) with 25 μL of rRABV or rRABV-MMP8 (20 FFU/mouse). The mortality of mice was monitored daily. At 2, 4, and 6 d.p.i., mice were euthanized with CO_2, and their brains were collected for RNA isolation and qPCR analysis. At 4 d.p.i., mice were euthanized with CO_2, and their brains were collected for cytometry.

qPCR. RNA was extracted with TRIzol reagent (Thermo Fisher, USA) and reverse transcribed with HiScript II Q RT SuperMix (Vazyme, Nanjing, China) to obtain cDNA. The quantitative real-time PCR (qPCR) volume was 10 μL, and the following cycling parameters were used: 95°C for 5 min, followed by 40 cycles at 95°C for 15 s and 60°C for 30 s. The transcript levels of targeted genes were calculated relative to the levels of β-actin using formula 2[cycle threshold (CT) (β-actin) – CT (target gene)]. The primers used in this study are listed in Table 1.

Western blotting. Brain tissues or cultured cells were lysed in radioimmunoprecipitation assay (RIPA) buffer, and the protein concentrations were determined using a bicinchoninic acid (BCA) protein assay kit (Beyotime, Shanghai, China). Equal quantities of total protein were resolved by 12% SDS-PAGE. Gels were transferred to polyvinylidene difluoride membranes (Bio-Rad, CA, USA) and subjected to Western blotting. The membranes were blocked with 5% nonfat milk and then incubated with a primary antibody and the corresponding horseradish peroxidase (HRP)-conjugated secondary antibody. The blots were then visualized with ECL reagent (Beyotime, Shanghai, China) and detected using an Amersham Imager 600 enhanced chemiluminescence (ECL) analysis system (GE, MA, USA).

Construction of promoter reporter plasmids. The MMP8 promoter reporter plasmids TSS-2500, TSS-2000, TSS-1500, TSS-1000, and TSS-500 containing the corresponding proximal promoter sequences of MMP8 were cloned by PCR amplification using genomic DNA of N2a cells as templates and subsequently cloned into PGL3-basic (Promega, Madison, WI, USA). The MMP8 promoter constructs containing site-specific mutations for the transcription factor binding site were constructed by overlap extension PCR. All constructs were verified by sequencing.

Promoter activity assay. N2a cells were cotransfected with 100 ng of full-length or a series of truncated or mutant promoter firefly luciferase reporter constructs and 10 ng of *Renilla* luciferase vector (pRL-TK). Luciferase activities were determined according to the manufacturer's protocol with a dual-luciferase reporter

assay system (Promega) and expressed as relative luciferase activity by normalizing firefly luciferase activity against *Renilla* luciferase activity.

Confocal microscopy. N2a cells seeded on 14-mm coverslips were transfected with plasmids, and the cells were infected or not with RABV. After incubation, the cells were fixed with 4% paraformaldehyde, permeabilized with 0.1% Triton X-100, and then stained with antibodies against c-Fos, p65, RABV-N, or 4′,6-diamidino-2-phenylindole (DAPI). After being washed three times, the cells were incubated with Alexa Fluor 488-conjugated or Alexa Fluor 594-conjugated secondary antibodies for 1 h at room temperature. Staining was visualized with a Zeiss LSM 880 confocal microscope under an oil objective (Carl Zeiss AG, Oberkochen, Germany).

ChIP. Chromatin immunoprecipitation (ChIP) assay was performed according to the manufacturer's protocol for the ChromaFlash high-sensitivity ChIP kit (Epigentek, Farmingdale, NY, USA). Briefly, N2a cells were transfected with pCAGGS-HA-c-Fos, pCAGGS-Flag-p65, or pCAGGS vector for 24 h and infected or not with RABV. Then the growth medium of N2a cells was removed, and cells were rinsed three times with cold PBS. Then cells were fixed with 1% formaldehyde for 15 min. Glycine was added to the cells to a final concentration of 125 mM to stop the cross-linking reaction. The cells were then sonicated to a fragment size range of 100 to 700 bp. Immunoprecipitation was performed by incubating sheared chromatin overnight at 4°C with HA tag or Flag tag antibodies. The ChIP DNA was then extracted, and 1/10 of the purified sample was subjected to PCR amplification with primer pairs spanning transcription factor binding sites. PCR products were resolved by 2% agarose gel electrophoresis and visualized using UV light. The expression level of a target DNA sequence was determined relative to its abundance in the input chromatin.

Immunofluorescence assay. bEnd.3 cells were seeded into a 24-well plate until reaching 100% confluence. After being treated with the indicated UV-inactivated brain supernatants for 48 h, the cells were fixed with 4% paraformaldehyde, permeabilized with 0.1% Triton X-100, and then stained with antibodies against ZO-1, occludin, and claudin-5, respectively. After being washed three times, the cells were incubated with Alexa Fluor 488-conjugated secondary antibodies for 1 h at room temperature. Then the cells were stained with DAPI. Fluorescent images were captured under an EVOS FL Auto (Thermo Fisher Scientific).

BBB integrity analysis. BBB permeability was determined by measuring sodium fluorescein (NaF) uptake as described previously, with minor modifications (48). Briefly, mice were injected with 100 μL of NaF (100 mg/mL) intraperitoneally. After 10 min to allow circulation of NaF, mice were anesthetized. Cardiac blood was collected, and brains were removed after mice were intracardially perfused with PBS. The fluorescence in serum and brain homogenate samples was analyzed by a FLUOstar Omega microplate reader (BMG Labtech, NC, USA) with excitation at 485 nm and emission at 530 nm. NaF uptake into tissue was calculated with the formula (micrograms of fluorescent brain/milligram of tissue)/(micrograms of fluorescent serum/milliliter of blood) to normalize values for blood levels of the dye at the time of tissue collection.

Transendothelial permeability assay. A transendothelial permeability assay was carried out as previously described (48). Briefly, bEnd.3 cells were seeded into 0.4-μm-pore-size Transwell filters until reaching 100% confluence. After being treated with the indicated UV-inactivated brain supernatants, fluorescein isothiocyanate (FITC)-dextran 10000 (10 kDa; Sigma-Aldrich, MO, USA) was added apically at 1 mg/mL for 30 min. Samples were removed from the lower chamber for fluorescence measurements (excitation, 492 nm; emission, 520 nm).

Isolation of leukocytes in the CNS. Leukocytes from the brains of mock-, rRABV-, and rRABV-MMP8-infected mice were isolated and analyzed. Mice were intracardially perfused with PBS. Brains were removed and digested with 1 μg/μL of collagenase D (no. 51657124; Roche, Germany) and 1 μg/μL of DNase I (no. 52779120; Roche) in Hanks balanced salt solution for 1 h to disperse the tissue into a single-cell suspension. Cells were then separated by discontinuous Percoll gradient (70/30%) centrifugation for 20 min (650 $\times$ *g* at room temperature, without brake). After being washed once with Hanks balanced salt solution, cells were stained for CD45 (30-F11, no. 553079), B220 (RA3-6B2, no. 561881), CD11b (M1/70, no. 557397), Ly6G (1A8, no. 560602), CD11c (N418, no. 565872), CD8 (53-6.7, no. 553032) (BD Pharmingen, CA, USA), CD45 (QA17A26, no. 157611), and CD4 (GK1.5, no. 100412) (Biolegend, CA, USA) with directly conjugated antibodies. Data collection and analysis were performed using a BD FACSVerse flow cytometer (BD Biosciences, CA, USA) and FlowJo software (TreeStar, CA, USA).

Statistical analysis. The graphs of Western blot and immunofluorescence results were analyzed using ImageJ software. The data were expressed as the means and standard deviations (SD). The Student *t* test was performed to analyze the significant differences between the two groups. One-way analysis of variance (ANOVA) was performed to analyze the significant differences between the three groups. The survival ratio was analyzed by a log rank (Mantel-Cox) test. The asterisks in figures indicate statistical significance (*, $P < 0.05$; **, $P < 0.01$; ***, $P < 0.001$). Graphs were plotted and analyzed using GraphPad Prism software, version 8.0 (GraphPad Software, La Jolla, CA, USA).

ACKNOWLEDGMENTS

This research was supported by the National Natural Science Foundation of China (31720103917 to Z.F.F. and 31872451 to L.Z.).

REFERENCES

1. World Health Organization. 2013. WHO Expert Consultation on Rabies. Second report. World Health Organization, Geneva, Switzerland.
2. Wang L, Cao Y, Tang Q, Liang G. 2013. Role of the blood-brain barrier in rabies virus infection and protection. Protein Cell 4:901–903. https://doi.org/10.1007/s13238-013-3918-8.
3. Schnell MJ, McGettigan JP, Wirblich C, Papaneri A. 2010. The cell biology of rabies virus: using stealth to reach the brain. Nat Rev Microbiol 8:51–61. https://doi.org/10.1038/nrmicro2260.
4. Willoughby RE, Jr, Tieves KS, Hoffman GM, Ghanayem NS, Amlie-Lefond CM, Schwabe MJ, Chusid MJ, Rupprecht CE. 2005. Survival after treatment

of rabies with induction of coma. N Engl J Med 352:2508–2514. https://doi.org/10.1056/NEJMoa050382.
5. Wang ZW, Sarmento L, Wang Y, Li XQ, Dhingra V, Tseggai T, Jiang B, Fu ZF. 2005. Attenuated rabies virus activates, while pathogenic rabies virus evades, the host innate immune responses in the central nervous system. J Virol 79:12554–12565. https://doi.org/10.1128/JVI.79.19.12554-12565.2005.
6. Hooper DC, Scott GS, Zborek A, Mikheeva T, Kean RB, Koprowski H, Spitsin SV. 2000. Uric acid, a peroxynitrite scavenger, inhibits CNS inflammation, blood-CNS barrier permeability changes, and tissue damage in a mouse model of multiple sclerosis. FASEB J 14:691–698. https://doi.org/10.1096/fasebj.14.5.691.
7. Kuang Y, Lackay SN, Zhao L, Fu ZF. 2009. Role of chemokines in the enhancement of BBB permeability and inflammatory infiltration after rabies virus infection. Virus Res 144:18–26. https://doi.org/10.1016/j.virusres.2009.03.014.
8. Hooper DC, Morimoto K, Bette M, Weihe E, Koprowski H, Dietzschold B. 1998. Collaboration of antibody and inflammation in clearance of rabies virus from the central nervous system. J Virol 72:3711–3719. https://doi.org/10.1128/JVI.72.5.3711-3719.1998.
9. Bennett J, Basivireddy J, Kollar A, Biron KE, Reickmann P, Jefferies WA, McQuaid S. 2010. Blood-brain barrier disruption and enhanced vascular permeability in the multiple sclerosis model EAE. J Neuroimmunol 229:180–191. https://doi.org/10.1016/j.jneuroim.2010.08.011.
10. Kean RB, Spitsin SV, Mikheeva T, Scott GS, Hooper DC. 2000. The peroxynitrite scavenger uric acid prevents inflammatory cell invasion into the central nervous system in experimental allergic encephalomyelitis through maintenance of blood-central nervous system barrier integrity. J Immunol 165:6511–6518. https://doi.org/10.4049/jimmunol.165.11.6511.
11. Faber M, Li J, Kean RB, Hooper DC, Alugupalli KR, Dietzschold B. 2009. Effective preexposure and postexposure prophylaxis of rabies with a highly attenuated recombinant rabies virus. Proc Natl Acad Sci U S A 106:11300–11305. https://doi.org/10.1073/pnas.0905640106.
12. Wang H, Zhang G, Wen Y, Yang S, Xia X, Fu ZF. 2011. Intracerebral administration of recombinant rabies virus expressing GM-CSF prevents the development of rabies after infection with street virus. PLoS One 6:e25414. https://doi.org/10.1371/journal.pone.0025414.
13. Abbott NJ, Patabendige AA, Dolman DE, Yusof SR, Begley DJ. 2010. Structure and function of the blood-brain barrier. Neurobiol Dis 37:13–25. https://doi.org/10.1016/j.nbd.2009.07.030.
14. Kadry H, Noorani B, Cucullo L. 2020. A blood-brain barrier overview on structure, function, impairment, and biomarkers of integrity. Fluids Barriers CNS 17:69. https://doi.org/10.1186/s12987-020-00230-3.
15. Liebner S, Dijkhuizen RM, Reiss Y, Plate KH, Agalliu D, Constantin G. 2018. Functional morphology of the blood-brain barrier in health and disease. Acta Neuropathol 135:311–336. https://doi.org/10.1007/s00401-018-1815-1.
16. Spindler KR, Hsu TH. 2012. Viral disruption of the blood-brain barrier. Trends Microbiol 20:282–290. https://doi.org/10.1016/j.tim.2012.03.009.
17. Candelario-Jalil E, Yang Y, Rosenberg GA. 2009. Diverse roles of matrix metalloproteinases and tissue inhibitors of metalloproteinases in neuroinflammation and cerebral ischemia. Neuroscience 158:983–994. https://doi.org/10.1016/j.neuroscience.2008.06.025.
18. Schubert-Unkmeir A, Konrad C, Slanina H, Czapek F, Hebling S, Frosch M. 2010. Neisseria meningitidis induces brain microvascular endothelial cell detachment from the matrix and cleavage of occludin: a role for MMP-8. PLoS Pathog 6:e1000874. https://doi.org/10.1371/journal.ppat.1000874.
19. Dallasta LM, Pisarov LA, Esplen JE, Werley JV, Moses AV, Nelson JA, Achim CL. 1999. Blood-brain barrier tight junction disruption in human immunodeficiency virus-1 encephalitis. Am J Pathol 155:1915–1927. https://doi.org/10.1016/S0002-9440(10)65511-3.
20. Strazza M, Pirrone V, Wigdahl B, Nonnemacher MR. 2011. Breaking down the barrier: the effects of HIV-1 on the blood-brain barrier. Brain Res 1399:96–115. https://doi.org/10.1016/j.brainres.2011.05.015.
21. Li F, Wang Y, Yu L, Cao S, Wang K, Yuan J, Wang C, Wang K, Cui M, Fu ZF. 2015. Viral infection of the central nervous system and neuroinflammation precede blood-brain barrier disruption during Japanese encephalitis virus infection. J Virol 89:5602–5614. https://doi.org/10.1128/JVI.00143-15.
22. Hsieh JT, Rathore APS, Soundarajan G, St John AL. 2019. Japanese encephalitis virus neuropenetrance is driven by mast cell chymase. Nat Commun 10:706. https://doi.org/10.1038/s41467-019-08641-z.
23. Roe K, Kumar M, Lum S, Orillo B, Nerurkar VR, Verma S. 2012. West Nile virus-induced disruption of the blood-brain barrier in mice is characterized by the degradation of the junctional complex proteins and increase in multiple matrix metalloproteinases. J Gen Virol 93:1193–1203. https://doi.org/10.1099/vir.0.040899-0.
24. Daniels BP, Holman DW, Cruz-Orengo L, Jujjavarapu H, Durrant DM, Klein RS. 2014. Viral pathogen-associated molecular patterns regulate blood-brain barrier integrity via competing innate cytokine signals. mBio 5:e01476-14. https://doi.org/10.1128/mBio.01476-14.
25. Wang PH, Dai JF, Bai FW, Kong KF, Wong SJ, Montgomery RR, Madri JA, Fikrig E. 2008. Matrix metalloproteinase 9 facilitates West Nile virus entry into the brain. J Virol 82:8978–8985. https://doi.org/10.1128/JVI.00314-08.
26. Ashley SL, Pretto CD, Stier MT, Kadiyala P, Castro-Jorge L, Hsu TH, Doherty R, Carnahan KE, Castro MG, Lowenstein PR, Spindler KR. 2017. Matrix metalloproteinase activity in infections by an encephalitic virus, mouse adenovirus type 1. J Virol 91:e01412-16. https://doi.org/10.1128/JVI.01412-16.
27. Chang CY, Li JR, Chen WY, Ou YC, Lai CY, Hu YH, Wu CC, Chang CJ, Chen CJ. 2015. Disruption of in vitro endothelial barrier integrity by Japanese encephalitis virus-infected astrocytes. Glia 63:1915–1932. https://doi.org/10.1002/glia.22857.
28. Chai Q, He WQ, Zhou M, Lu H, Fu ZF. 2014. Enhancement of blood-brain barrier permeability and reduction of tight junction protein expression are modulated by chemokines/cytokines induced by rabies virus infection. J Virol 88:4698–4710. https://doi.org/10.1128/JVI.03149-13.
29. Phares TW, Fabis MJ, Brimer CM, Kean RB, Hooper DC. 2007. A peroxynitrite-dependent pathway is responsible for blood-brain barrier permeability changes during a central nervous system inflammatory response: TNF-alpha is neither necessary nor sufficient. J Immunol 178:7334–7343. https://doi.org/10.4049/jimmunol.178.11.7334.
30. Barkhouse DA, Garcia SA, Bongiorno EK, Lebrun A, Faber M, Hooper DC. 2015. Expression of interferon gamma by a recombinant rabies virus strongly attenuates the pathogenicity of the virus via induction of type I interferon. J Virol 89:312–322. https://doi.org/10.1128/JVI.01572-14.
31. Phares TW, Kean RB, Mikheeva T, Hooper DC. 2006. Regional differences in blood-brain barrier permeability changes and inflammation in the apathogenic clearance of virus from the central nervous system. J Immunol 176:7666–7675. https://doi.org/10.4049/jimmunol.176.12.7666.
32. Lebrun A, Portocarrero C, Kean RB, Barkhouse DA, Faber M, Hooper DC. 2015. T-bet is required for the rapid clearance of attenuated rabies virus from central nervous system tissue. J Immunol 195:4358–4368. https://doi.org/10.4049/jimmunol.1501274.
33. Roy A, Phares TW, Koprowski H, Hooper DC. 2007. Failure to open the blood-brain barrier and deliver immune effectors to central nervous system tissues leads to the lethal outcome of silver-haired bat rabies virus infection. J Virol 81:1110–1118. https://doi.org/10.1128/JVI.01964-06.
34. Luo J, Zhang B, Wu Y, Tian Q, Mo M, Long T, Mei M, Fan R, Lyu Z, Jiang H, Wu F, Lin Y, Guo X. 2018. Recombinant rabies virus expressing interleukin-6 enhances the immune response in mouse brain. Arch Virol 163:1889–1895. https://doi.org/10.1007/s00705-018-3808-8.
35. Stamatovic SM, Keep RF, Kunkel SL, Andjelkovic AV. 2003. Potential role of MCP-1 in endothelial cell tight junction 'opening': signaling via Rho and Rho kinase. J Cell Sci 116:4615–4628. https://doi.org/10.1242/jcs.00755.
36. Chai Q, She R, Huang Y, Fu ZF. 2015. Expression of neuronal CXCL10 induced by rabies virus infection initiates infiltration of inflammatory cells, production of chemokines and cytokines, and enhancement of blood-brain barrier permeability. J Virol 89:870–876. https://doi.org/10.1128/JVI.02154-14.
37. Gnanadurai CW, Fu ZF. 2016. CXCL10 and blood-brain barrier modulation in rabies virus infection. Oncotarget 7:10694–10695. https://doi.org/10.18632/oncotarget.7428.
38. Yu F, Zhang G, Zhong X, Han N, Song Y, Zhao L, Cui M, Rayner S, Fu ZF. 2014. Comparison of complete genome sequences of dog rabies viruses isolated from China and Mexico reveals key amino acid changes that may be associated with virus replication and virulence. Arch Virol 159:1593–1601. https://doi.org/10.1007/s00705-013-1966-2.
39. Sui B, Chen D, Liu W, Tian B, Lv L, Pei J, Wu Q, Zhou M, Fu ZF, Zhang Y, Zhao L. 7 December 2021. Comparison of lncRNA and mRNA expression in mouse brains infected by a wild-type and a lab-attenuated Rabies lyssavirus. J Gen Virol https://doi.org/10.1099/jgv.0.001538.
40. Liu XQ, Su P, Meng SS, Aschner M, Cao YP, Luo WJ, Zheng G, Liu MC. 2017. Role of matrix metalloproteinase-2/9 (MMP2/9) in lead-induced changes in an in vitro blood-brain barrier model. Int J Biol Sci 13:1351–1360. https://doi.org/10.7150/ijbs.20670.
41. Zhang Q, Zheng M, Betancourt CE, Liu LF, Sitikov A, Sladojevic N, Zhao Q, Zhang JH, Liao JMK, Wu RX. 2021. Increase in blood-brain barrier (BBB) permeability is regulated by MMP3 via the ERK signaling pathway. Oxid Med Cell Longev 2021:6655122. https://doi.org/10.1155/2021/6655122.
42. Nichols P, Urriola J, Miller S, Bjorkman T, Mahady K, Vegh V, Nasrallah F, Winter C. 2021. Blood-brain barrier dysfunction significantly correlates with serum matrix metalloproteinase-7 (MMP-7) following traumatic brain injury. Neuroimage Clin 31:102741. https://doi.org/10.1016/j.nicl.2021.102741.

43. Chelluboina B, Klopfenstein JD, Pinson DM, Wang DZ, Vemuganti R, Veeravalli KK. 2015. Matrix metalloproteinase-12 induces blood-brain barrier damage after focal cerebral ischemia. Stroke 46:3523–3531. https://doi.org/10.1161/STROKEAHA.115.011031.
44. Lee EJ, Han JE, Woo MS, Shin JA, Park EM, Kang JL, Moon PG, Baek MC, Son WS, Ko YT, Choi JW, Kim HS. 2014. Matrix metalloproteinase-8 plays a pivotal role in neuroinflammation by modulating TNF-alpha activation. J Immunol 193:2384–2393. https://doi.org/10.4049/jimmunol.1303240.
45. Nakamichi K, Saiki M, Sawada M, Takayama-Ito M, Yamamuro Y, Morimoto K, Kurane I. 2005. Rabies virus-induced activation of mitogen-activated protein kinase and NF-kappaB signaling pathways regulates expression of CXC and CC chemokine ligands in microglia. J Virol 79:11801–11812. https://doi.org/10.1128/JVI.79.18.11801-11812.2005.
46. Karin M. 1998. Mitogen-activated protein kinase cascades as regulators of stress responses. Ann N Y Acad Sci 851:139–146. https://doi.org/10.1111/j.1749-6632.1998.tb08987.x.
47. Solan PD, Dunsmore KE, Denenberg AG, Odoms K, Zingarelli B, Wong HR. 2012. A novel role for matrix metalloproteinase-8 in sepsis. Crit Care Med 40:379–387. https://doi.org/10.1097/CCM.0b013e318232e404.
48. Luo Z, Lv L, Li Y, Sui B, Wu Q, Zhang Y, Pei J, Li M, Zhou M, Hooper DC, Fu ZF, Zhao L. 2020. Dual role of Toll-like receptor 7 in the pathogenesis of rabies virus in a mouse model. J Virol 94:e00111-20. https://doi.org/10.1128/JVI.00111-20.
49. Shih MF, Pan KH, Cherng JY. 2015. Possible mechanisms of di(2-ethylhexyl) phthalate-induced MMP-2 and MMP-9 expression in A7r5 rat vascular smooth muscle cells. Int J Mol Sci 16:28800–28811. https://doi.org/10.3390/ijms161226131.
50. Cheng G, Wei L, Xiurong W, Xiangzhen L, Shiguang Z, Songbin F. 2009. IL-17 stimulates migration of carotid artery vascular smooth muscle cells in an MMP-9 dependent manner via p38 MAPK and ERK1/2-dependent NF-kappaB and AP-1 activation. Cell Mol Neurobiol 29:1161–1168. https://doi.org/10.1007/s10571-009-9409-z.
51. Woo CH, Lim JH, Kim JH. 2004. Lipopolysaccharide induces matrix metalloproteinase-9 expression via a mitochondrial reactive oxygen species-p38 kinase-activator protein-1 pathway in Raw 264.7 cells. J Immunol 173:6973–6980. https://doi.org/10.4049/jimmunol.173.11.6973.
52. Tian B, Zhou M, Yang Y, Yu L, Luo Z, Tian D, Wang K, Cui M, Chen H, Fu ZF, Zhao L. 2017. Lab-attenuated rabies virus causes abortive infection and induces cytokine expression in astrocytes by activating mitochondrial antiviral-signaling protein signaling pathway. Front Immunol 8:2011. https://doi.org/10.3389/fimmu.2017.02011.
53. Embregts CWE, Begeman L, Voesenek CJ, Martina BEE, Koopmans MPG, Kuiken T, GeurtsvanKessel CH. 2021. Street RABV induces the cholinergic anti-inflammatory pathway in human monocyte-derived macrophages by binding to nAChr α7. Front Immunol 12:622516. https://doi.org/10.3389/fimmu.2021.622516.
54. Huber JD, Egleton RD, Davis TP. 2001. Molecular physiology and pathophysiology of tight junctions in the blood-brain barrier. Trends Neurosci 24:719–725. https://doi.org/10.1016/s0166-2236(00)02004-x.
55. Rempe RG, Hartz AMS, Bauer B. 2016. Matrix metalloproteinases in the brain and blood-brain barrier: versatile breakers and makers. J Cereb Blood Flow Metab 36:1481–1507. https://doi.org/10.1177/0271678X16655551.
56. Zhang Y, Fan F, Zeng G, Zhou L, Zhang Y, Zhang J, Jiao H, Zhang T, Su D, Yang C, Wang X, Xiao K, Li H, Zhong Z. 2017. Temporal analysis of blood-brain barrier disruption and cerebrospinal fluid matrix metalloproteinases in rhesus monkeys subjected to transient ischemic stroke. J Cereb Blood Flow Metab 37:2963–2974. https://doi.org/10.1177/0271678X16680221.
57. Gerwien H, Hermann S, Zhang XL, Korpos E, Song J, Kopka K, Faust A, Wenning C, Gross CC, Honold L, Melzer N, Opdenakker G, Wiendl H, Schafers M, Sorokin L. 2016. Imaging matrix metalloproteinase activity in multiple sclerosis as a specific marker of leukocyte penetration of the blood-brain barrier. Sci Transl Med 8:364ra152. https://doi.org/10.1126/scitranslmed.aaf8020.
58. Tasaki A, Shimizu F, Sano Y, Fujisawa M, Takahashi T, Haruki H, Abe M, Koga M, Kanda T. 2014. Autocrine MMP-2/9 secretion increases the BBB permeability in neuromyelitis optica. J Neurol Neurosurg Psychiatry 85:419–430. https://doi.org/10.1136/jnnp-2013-305907.
59. Eugenin EA, Osiecki K, Lopez L, Goldstein H, Calderon TM, Berman JW. 2006. CCL2/monocyte chemoattractant protein-1 mediates enhanced transmigration of human immunodeficiency virus (HIV)-infected leukocytes across the blood-brain barrier: a potential mechanism of HIV-CNS invasion and NeuroAIDS. J Neurosci 26:1098–1106. https://doi.org/10.1523/JNEUROSCI.3863-05.2006.
60. Louboutin JP, Agrawal L, Reyes BA, Van Bockstaele EJ, Strayer DS. 2010. HIV-1 gp120-induced injury to the blood-brain barrier: role of metalloproteinases 2 and 9 and relationship to oxidative stress. J Neuropathol Exp Neurol 69:801–816. https://doi.org/10.1097/NEN.0b013e3181e8c96f.
61. Kumar H, Jo MJ, Choi H, Muttigi MS, Shon S, Kim BJ, Lee SH, Han IB. 2018. Matrix metalloproteinase-8 inhibition prevents disruption of blood-spinal cord barrier and attenuates inflammation in rat model of spinal cord injury. Mol Neurobiol 55:2577–2590. https://doi.org/10.1007/s12035-017-0509-3.
62. Han JE, Lee EJ, Moon E, Ryu JH, Choi JW, Kim HS. 2016. Matrix metalloproteinase-8 is a novel pathogenetic factor in focal cerebral ischemia. Mol Neurobiol 53:231–239. https://doi.org/10.1007/s12035-014-8996-y.
63. Li Y, Zhou M, Luo Z, Zhang Y, Cui M, Chen H, Fu ZF, Zhao L. 2017. Overexpression of interleukin-7 extends the humoral immune response induced by rabies vaccination. J Virol 91:e02324-16. https://doi.org/10.1128/JVI.02324-16.
64. Sui B, Chen D, Liu W, Wu Q, Tian B, Li Y, Hou J, Liu S, Xie J, Jiang H, Luo Z, Lv L, Huang F, Li R, Zhang C, Tian Y, Cui M, Zhou M, Chen H, Fu ZF, Zhang Y, Zhao L. 2020. A novel antiviral lncRNA, EDAL, shields a T309 O-GlcNAcylation site to promote EZH2 lysosomal degradation. Genome Biol 21:228. https://doi.org/10.1186/s13059-020-02150-9.